Journal of Electronic Materials (2022) 51:5368–5375
https://doi.org/10.1007/s11664-022-09775-5

ORIGINAL RESEARCH ARTICLE

Dielectric Studies of Nano-Magnesium Silicate and Linear Low-Density Polyethylene Composite As a Substrate for High-Frequency Applications

Pulin Dutta[1] · **Kunal Borah**[1]

Received: 3 December 2021 / Accepted: 14 June 2022 / Published online: 4 July 2022
© The Minerals, Metals & Materials Society 2022

Abstract
Dielectric properties of a magnesium silicate ($MgSiO_3$) linear low-density polyethylene nanocomposite are studied in the X-band frequencies to realize its application as a substrate for high-frequency devices. $MgSiO_3$ ceramics are synthesized by conventional solid state technique. Structural and morphological characteristics of $MgSiO_3$ nanoparticles are confirmed by X-ray diffraction, Fourier transform infrared spectroscopy and transmission electron microscopy. Transmission electron microscopy images reveal the average particle size to be ~100 nm. Composites are prepared by uniform dispersion of the nano-inclusions $MgSiO_3$ in a linear low-density polyethylene matrix in three different wt.%, viz. 2%, 4% and 6%. The fractured lateral side of the composite is examined under a scanning electron microscope to ensure the uniform dispersion of the inclusions in the polymer. Water absorption measurement is carried out based on ASTM D570-98. Densities of the samples are measured by hydrostatic weighing by using Archimedes principle. Thermal conductivity of the composites is measured by modified hot plat method. Nicholson-Ross approach is used to investigate the dielectric characteristics of composites. The permittivity and dielectric loss tangent of the nano-composite in the X-band are found to be ~2.2–2.5 and 10^{-2}–10^{-4} for all the inclusion concentration respectively. To see the applicability of the nanocomposite in the field of antenna, return losses are calculated from complex permittivity and complex permittivity data.

Keywords Complex permittivity · complex permeability · return loss · X-band

Introduction

The main concern for electronic devices with the development of modern electronic industries is substrates with specific properties for high-frequency operation.[1] The key factors that determine the capability of a material to be used in high-frequency microwave devices are its complex permittivity and complex permeability. Since a single material may not always be able to meet all the requirements for a specific application, composites such as a polymer matrix with inclusions of various types (nano, ceramic, magnetic etc.) could be a good choice.[2] Dielectric ceramics have good dielectric strength, low dielectric constant and low loss tangent,[3] which ensures that composites of polymer-dielectric ceramic nanomaterials can be potential substrate materials for different types of microwave applications.

Many ceramic nanomaterials such as Mg_2SiO_4, $Ba(Mg_{1/3}Ta_{2/3})O_3$, $Mg_4Nb_2O_9$, and $ZnAl_2O_4$ have been reported so far because of their suitable microwave dielectric properties.[4] Nano-ceramic-PTFE composite and fiberglass polymer resin composites are used for high-frequency microwave substrate applications.[5] In Ref. 6 Silicon rubber-$BaBiLiTeO_6$ ceramic polymer composite substrate is reported for 5G applications. The composites reported the complex permittivity (ε') and loss tangent ($\tan \delta_e$) are 6.86 and 4.7 $\times 10^{-2}$, respectively, at 10 GHz. In Ref. 7 dielectric properties of TiO_2-polyolefin-based composite are investigated. For 70 wt% filler loading, the reported values of ε' and $\tan \delta_e$ are 7.03 and 4.2×10^{-3}, respectively. In Ref. 8 Dielectric properties of PTFE loaded with varying %VF of $MgTiO_3$ are studied. The measured value of ε' is 5.5 and $\tan \delta_e = 2.7\times 10^{-4}$ (at 10 GHz), making the composite a promising material for

✉ Kunal Borah
kbnerist@gmail.com

[1] Department of Physics, North Eastern Regional Institute of Science and Technology (Deemed-to-be-University), Nirjuli, Itanagar, Arunachal Pradesh 791109, India

electronic packaging. Dielectric properties of $CaTiO_3$ -loaded polypropylene composite fabricated through compression molding are studied using X-band cavity perturbation for microwave substrate application.[9] The composite has an effective ε' and tan δ_e is 11.74 and 7×10^{-3} , respectively, for the highest filler concentration. Dielectric properties of PTFE composites filled with perovskite (Ca,Li,Sm)TiO_3 (CLST) dielectric ceramic with volume fractions up to 60% are prepared and studied at 10 GHz.[10] The obtained ε' and tan δ_e is 5.5 and 2.7×10^{-4} for optimum filler loading makes it a promising material in the electronic packaging field. In Ref. 11 Si_3N_4 -filled PTFE composites is prepared for composites for substrates at microwave frequencies. At 62 %VF of Si_3N_4 ceramic filler, the prepared Si_3N_4/PTFE composite exhibits excellent low ε' and tan δ_e , and the values are 4.03 and 1.4×10^{-3} , respectively. A low-density polyethylene (LDPE)-nano-titania (TiO_2) composite with $\varepsilon' = 2.4$ and tan $\delta = 4\times10^{-3}$ has been reported as substrate for X-band devices.[12] It is also reported in Ref. 12 that the bandwidth and S11 of the device can be further enhanced by the use of a graded composite as substrate material. Moreover, a frequency-independent behaviour of complex permittivity is reported in a comparative study of dielectric behaviour for different composites at the X-band.[13] The composites used are nano-barium titanate ($BaTiO_3$) inclusions in two different polymer matrices, namely, polyaniline (PANI) powder and maleic resin. In Ref. 14 microstrip patch antennas are fabricated over composites of polyvinyl chloride with nano-barium titanate ($\varepsilon' = 37$) and nano-neodymium titanate ($\varepsilon' = 85$) inclusions. A modified W-shaped Ka band antenna on an Al_2O_3 ceramic substrate with $\varepsilon' = 7$ is presented in Ref. 15. In Ref. 16 a circular patch monopole antenna on a high permittivity ceramic polytetrafluoroethylene (PTFE) composite with $\varepsilon' = 6.3$ is reported with enhanced radiation characteristics. In Ref. 17 a rectangular microstrip patch antenna is designed on a $(Zn_{0.7}Mg_{0.3})TiO_3$ ceramic dielectric substrate with $\varepsilon' = 21.3$. In Ref. 18 $(Bi_{13}Co_{11})Co_2O_{40}$-$Co_3O_4$ ceramic nanocomposite is synthesized and widely researched for application as a microstrip patch antenna (MPA) substrate. The reported ε' and tan δ of the material are 6.58 and 2×10^{-4} , respectively.

In this paper, nano-$MgSiO_3$ is synthesized and used as inclusions in a linear low-density polyethylene (LLDPE) polymer matrix. LLDPE is a polymer with linear characteristics and acceptable electrical properties, good tensile properties significant resistance to chemicals, low water absorbance and high thermal stability. The decomposition temperature of LLDPE is 438.85°C with weight loss of 0.01%. The major weight loss occurs between the temperatures 441.98° and 513.15°C due to growth of volatiles.[19–21] The softening temperature of LLDPE is ~85°C.[22] Measurements of complex permittivity and permeability of the composites (LLDPE-nano-$MgSiO_3$) with 2, 4, and 6 wt.% of $MgSiO_3$ with in LLDPE polymer matrix is performed in the X-band.

Experimental Work

Synthesis of Nano-$MgSiO_3$ and LLDPE-Nano-$MgSiO_3$ Composite Substrates

$MgSiO_3$ nanoparticles are synthesized by conventional solid-state method[23] by using high-purity (>99%) oxides MgO and SiO_2. Firstly, MgO and SiO_2 (Sigma Aldrich) powders are ball milled for 5 h. After drying, the MgO and SiO_2 powders are mixed uniformly and calcined at 1200°C for 8 h. The powders are then ball milled again for another 2 h before drying to obtain the nanoparticles. To fabricate the composite for complex permittivity and permeability characterization, LLDPE is first dissolved in toluene and stirred using a mechanical stirrer at 100°C. After dissolving, the desired wt.% (2, 4 and 6) of the synthesized $MgSiO_3$ nanoparticles are added to make a homogenous mixture of the inclusions in the polymer. A viscous solution is obtained when toluene completely evaporates. The solution is then poured into a die with dimensions $10 \times 22 \times 2$ mm^3, and left to congeal for 2 h at room temperature, and a composite substrate of LLDPE-nano-$MgSiO_3$ is thus obtained.[24] Further, it is observed that beyond 6 wt.%, the ductility of the substrate decreases.

Structural and Morphological Characterization

X-ray diffraction (XRD) patterns of the synthesized $MgSiO_3$ nanoparticles are shown in Fig. 1 recorded by using a Bruker D8 (Make: BRUKER AXS, GERMANY, Model: D8

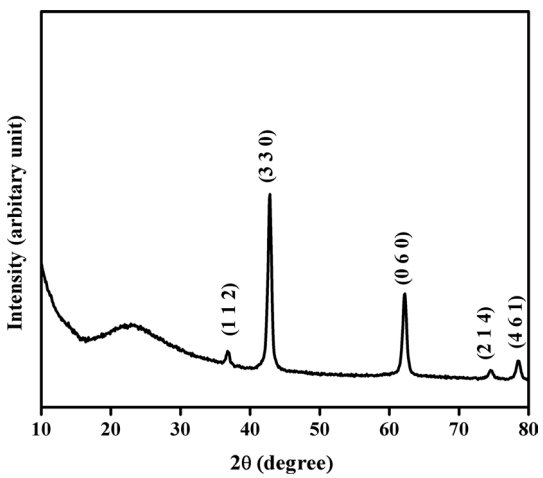

Fig. 1 XRD of magnesium silicate.

FOCUS) X-ray powder diffractometer using Cu Kα radiation ($\lambda = 1.5406$ Å). The peaks at $2\theta = 36.81°$, 42.80°, 62.16°, 74.56° and 78.47° corresponding to the (*h k l*) value (1 1 2), (3 3 0), (0 6 0), (2 1 4), (4 6 4) are the diffraction peaks of $MgSiO_3$ (ICDD 01-074-2017). A thorough examination of the pattern reveals that the sample has an orthorhombic structure having lattice parameters: $a = 4.7450$ Å, $b = 4.9070$ Å, $c = 6.8530$ Å.

Fourier transform infrared (FTIR) spectra of nano-$MgSiO_3$ is recorded using a NICOLET FTIR spectrometer in 400–4000 cm^{-1} range (Make: NICOLET, model: IMPACT 410). FTIR spectra are obtained by mixing the sample with KBr and grinding to a very fine powder. The FTIR spectrum of the synthesized $MgSiO_3$ is shown in Fig. 2. The -OH stretching vibration caused by physical adsorption of water and bound water is responsible for the broad characteristic band ranging from 3770 cm^{-1} to 2480 cm^{-1} in Fig. 2. The stretching vibration of zeolite water causes the distinctive band at 1641 cm^{-1}. The distinctive bands at 1186–1047 cm^{-1} belong to Si-O bending vibrations, whereas the band at 480 cm^{-1} correlates to Mg-O stretching vibrations.

To confirm the average particle size of the synthesized nanomaterial, a transmission electron microscope (TEM) (Model: TECNAI G2 20 S-TWIN Make: FEI COMPANY, USA) is used. The TEM image shown in Fig. 3 reveals that the average particle size of synthesized nano-$MgSiO_3$ is ~100 nm. To confirm the uniform distribution of $MgSiO_3$ in LLDPE composite substrates, the lateral side of fractured samples of 6 wt% is scanned via a scanning electron microscope (SEM) (Model: JSM- 35CF,Make: JEOL). The SEM images of LLDPE-nano-$MgSiO_3$ composite substrates are shown in Fig. 4. It is observed that clustering of inclusions formed in the composite (shown in the inset of Fig. 4), which is due to the high viscosity of LLDPE. It is confirmed from the SEM images that $MgSiO_3$ nanoparticles are uniformly distributed in the LLDPE matrix.

Material properties may change under the influence of adverse environmental conditions such as high moisture or humidity. So properties such as water absorbance, density, thermal conductivity, coefficient of thermal expansion (CTE) must be explored. Water absorption measurement is carried out based on ASTM D570-98 and as shown in Fig. 5. For this increase in wt% of pure LLDPE and the composites (2, 4 and 6%), a sample of size $10 \times 22 \times 2$ mm^3 is measured after immersing in distilled water. At first, weights of the dry composite is measured. Then, at room temperature, identical pieces of pure LLDPE and composites are dipped in distilled water. After soaking for 24 h, the samples are removed from water and the weight is recorded. This procedure is repeated until saturation is

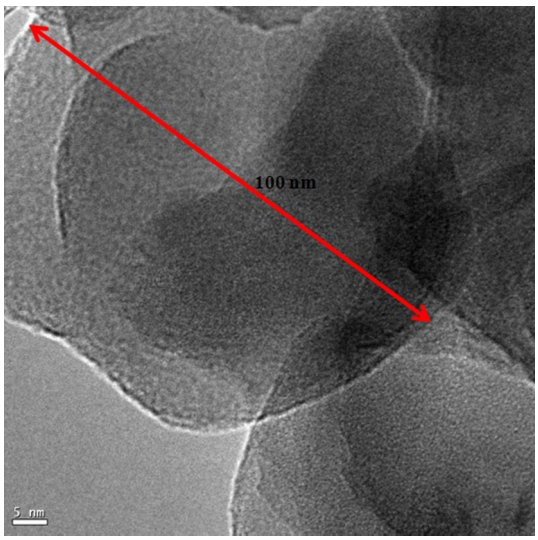

Fig. 3 TEM of magnesium silicate.

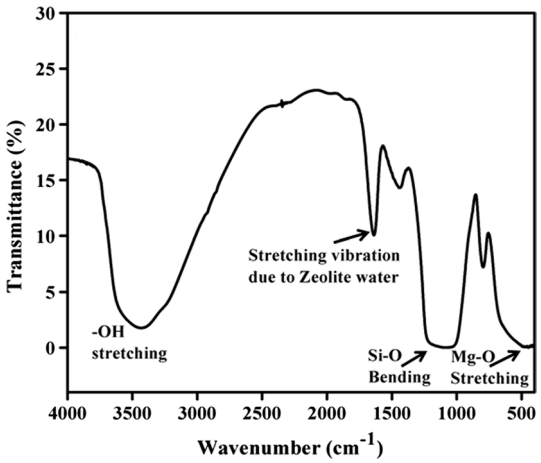

Fig. 2 FTIR of magnesium silicate.

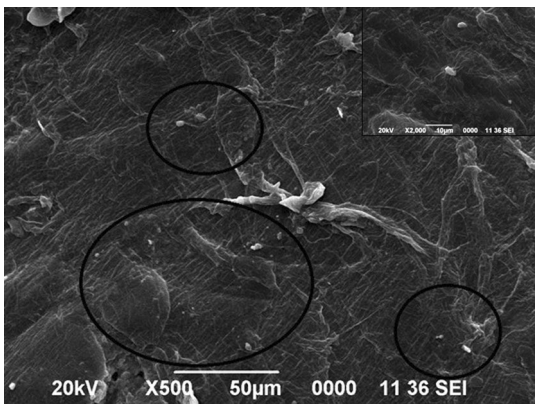

Fig. 4 SEM of LLDPE-nano-$MgSiO_3$ (6%) composite.

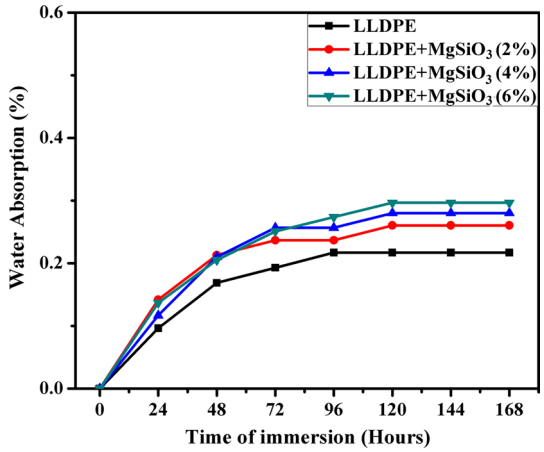

Fig. 5 Water absorbance of pure LLDPE and LLDPE-nano-$MgSiO_3$ composite.

Table I Water absorbance data for the LLDPE-nano-$MgSiO_3$ composite substrate

Sample (wt.%)	Water Absorption (in.%)
LLDPE	0.21
LLDPE+$MgSiO_3$ (2%)	0.26
LLDPE+$MgSiO_3$ (4%)	0.28
LLDPE+$MgSiO_3$ (6%)	0.29

achieved.[25] The percentage of water absorption is calculated by using the expression given below

$$w_a(\text{in }\%) = \frac{w_f - w_i}{w_i} \times 100 \tag{1}$$

where w_a = percentage of absorbing water. w_f = final weight of the pieces. w_i = initial weight of the pieces.

From the water absorption graph it is seen that the saturation for all the samples are obtained after 168 h of immersion. The saturated water absorption values is given in Table I.

Densities of the samples are measured by hydrostatic weighing by using the Archimedes principle. For this, a beaker that is partially filled with ethanol is placed on balance and the combined mass of the beaker is measured (w_1). Then the composite sample is suspended in the ethanol and the new reading is taken (w_2). Finally, the sample is allowed to settle on the bottom of the beaker and a reading is taken (w_3).[26] By using the value of w_1 w_2 w_3 and d (density of ethanol), the density is measured by using the following expression

Table II Density of nano-$MgSiO_3$-LLDPE composite substrate

Sample (wt.%)	Density (g/cm^3)
LLDPE	0.92
LLDPE+$MgSiO_3$ (2%)	0.98
LLDPE+$MgSiO_3$ (4%)	1.04
LLDPE+$MgSiO_3$ (6%)	1.12

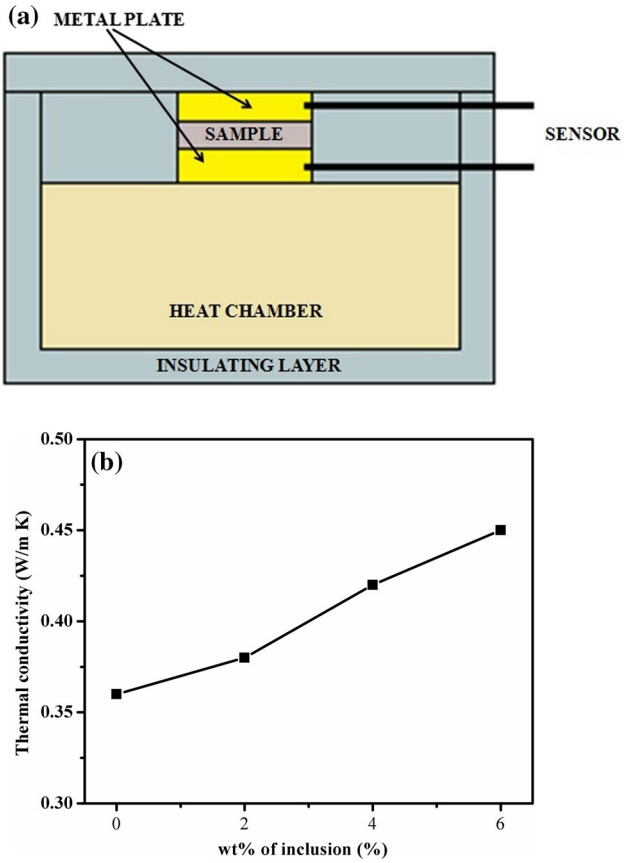

Fig. 6 (a) Schematic of insulated chamber for heat application. (b) Thermal conductivity as a function of wt% of inclusion.

$$\rho = \frac{w_3 - w_1}{w_2 - w_1} \times d\left(\text{g/cm}^3\right) \tag{2}$$

The obtained value of density is listed in Table II.

The thermal conductivity of pure LLDPE and the composites are measured by a modified heat flow meter. The experimental setup consists of a sample holder with insulated chamber for heat application, heat sensors and an interfacing computer for data acquisition. The schematic is shown in Fig. 6a. For measurement, a sample of dimensions $3 \times 3 \times 0.02$ cm^2 is inserted between a hot plate and a cold plate, and the thermal conductivity is determined once the steady-state is achieved by applying Fourier's law[27] expressed as

$$\frac{Q}{A} = k\frac{T_h - T_c}{x} \tag{3}$$

where Q/A is heat flow per unit area, k is the thermal conductivity, x is the thickness of the sample, T_h is the hot surface temperature, T_c is the cold surface temperature

The calculated value of thermal conductivity of pure LLDPE and the composites are shown in the Table III. The thermal conductivity of LLDPE is very low because of the strong C-H bond and absence of free electrons, although heat transfer is observed due to vibrations of the bond. As the percentage of inclusion increases, the value of thermal conductivity increases due to the relatively higher thermal conductivity of $MgSiO_3$ than LLDPE. The increase in thermal conductivity as a function of filler wt.% is shown in Fig. 6b. The increasing trend in thermal conductivity due to filler loading is minimal due to the low filler increase.

The coefficient of thermal expansion (CTE) is a crucial feature that must be investigated further. CTE is determined using the mixing rule, which states that the CTE of a two-phase composite is directly proportional to the wt.% of the filler.[28] The mixing rule is stated as follows:

$$\alpha_c = f\ \alpha_f + (1-f)\alpha_m \tag{4}$$

where α_f, α_m and α_c are the filler, matrix and composite, and CTEs, respectively, and f is the filler volume percent. Table IV shows the computed CTE values.

Dielectric Characterization

The Nicholson–Ross approach[29] is used to calculate complex permittivity and permeability at the X-band. An Agilent WR-90 X11644A rectangular waveguide line, an Agilent E8362C vector network analyzer, sample container of $\lambda/4$ thickness, and an interfacing computer are used in the measurement setup. Prior to measurements, the system was calibrated using the through–reflect–line (TRL) approach to reduce any inaccuracies.[30] Following TRL calibration, LLDPE-nano-$MgSiO_3$ composite substrates of 10 ×22 × 2 mm^3 are placed into the sample holder to obtain complex permittivity and permeability.

Table III Thermal conductivity of nano-$MgSiO_3$-LLDPE composite substrate

Sample (wt.%)	Thermal conductivity (W/m K)
LLDPE	0.36
LLDPE+$MgSiO_3$ (2%)	0.39
LLDPE+$MgSiO_3$ (4%)	0.41
LLDPE+$MgSiO_3$ (6%)	0.45

The real part of complex permittivity (ε') and dielectric loss tangent (tan δ_e) of LLDPE-nano-$MgSiO_3$ for the considered wt.% in the X-band microwave frequency at room temperature is shown in Fig. 7a and b. Pure LLDPE and $MgSiO_3$ have a ε' of 2.2 and 6.4.[17] The standard error of ε' and tan δ_e from its mean is depicted as the error bars in the plots of Fig. 7a and b. The deviations observed are due to various reasons such as casting pressure and formation of agglomerated of the inclusions in the polymer matrix. The real part of complex permittivity (ε') is found to be almost constant over the X-band frequency range. The average

Table IV Coefficient of thermal expansion of nano-$MgSiO_3$-LLDPE composite substrate

Material (wt.%)	CTE (k^{-1})
LLDPE	18×10^{-5}
$MgSiO_3$	2.44×10^{-5}
LLDPE+ $MgSiO_3$ (2%)	17.6888×10^{-5}
LLDPE+ $MgSiO_3$ (4%)	17.3776×10^{-5}
LLDPE+ $MgSiO_3$ (6%)	17.0664×10^{-5}

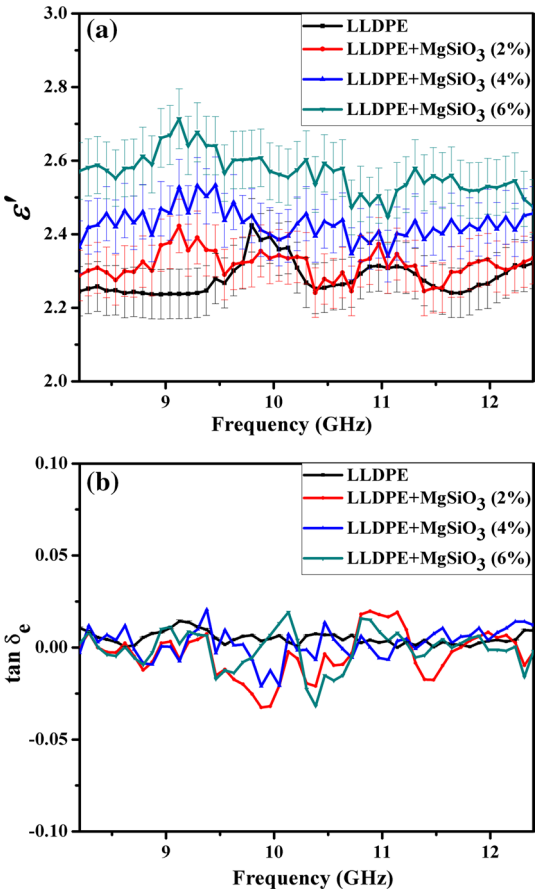

Fig. 7 (a) Real part of complex permittivity and (b) Dielectric loss tangent of LLDPE-nano-$MgSiO_3$composites.

values of real permittivity of the composite with 2, 4 and 6 wt.% inclusion content are 2.31, 2.42 and 2.56, respectively. Since the wt.% variances of inclusions in the host matrix are minimal, the change in ε' is also minor. Because of intrinsic electric dipole polarization and interfacial polarization, permittivity of the composite substrate increases as the inclusion content is increased. The polarization in $MgSiO_3$ is because of the presence of Mg^{2+} ions. As Mg^{2+} ions are strongly polarizable, increase in Mg^{2+} ions as inclusion concentration increases, enhances the total permittivity of the composite.[31] A slight non-linear behaviour is observed in the complex permittivity measurements due to space charge accumulation at the multiple interfaces formed as a result of heterogeneous composite system of dispersant $MgSiO_3$ in the LLDPE matrix.[32]

Figure 7b depicts the dielectric loss tangent, tan δ_e, of the composite LLDPE-nano-$MgSiO_3$. Dielectric loss essentially relates to two forms of energy dissipation, namely conduction loss and dielectric loss. Prospective dielectric substance has low energy loss as heat. The tan δ_e values of the composite LLDPE-nano-$MgSiO_3$ appears to range between 10^{-2} and 10^{-4} with frequency. Because of the coupling effect of the host matrix and inclusion in the Fabry–Perot resonance (FPR) region, negative values of tan δ_e in the X-band are observed.[33] Negative loss tangent values are not necessarily an inherent property of the material, as they also depend on the thickness of the substrate.[34] Corresponding FPR can readily alter the linked electromagnetic field if the substrate thickness is $\lambda/2$. In this investigation, a sample holder thickness of $\lambda/4$ is considered. In their studies, Axelrod et al. explain this unusual behaviour. According to the study, when more energy is emitted than absorbed at a specific frequency, a negative loss phenomenon is seen. The total energy of the sample must be conserved according to the principle of conservation of energy. The non-compensated matrix-anchored charges inside the polymer matrix and on the interface is responsible for the negative loss phenomenon. Non-bonding orbitals, full or empty for positive and negative ions, may generate charge anchoring, which facilitates charge separation. As a result, the molecules achieve a metastable state in which charge separation causes energy accumulation. Conditions such as frequency and temperature can remove this metastable state. Charge avalanche recombination may occur at the required temperature and frequency, resulting in energy release.[35]

The real part of complex permeability (μ') and loss tangent (tan δ_m) for 2, 4 and 6 wt.% of LLDPE-nano-$MgSiO_3$ composite is shown in Fig. 8a and b. The figure shows the standard deviation of μ' and tan δ_m from its mean value. Increasing inclusion content in the host matrix reduces the average value of μ' from 1.07 to 1.04. This might have been caused by the presence of non-magnetic $MgSiO_3$ in the non-magnetic polymer host matrix, which lowers intergranular magnetic

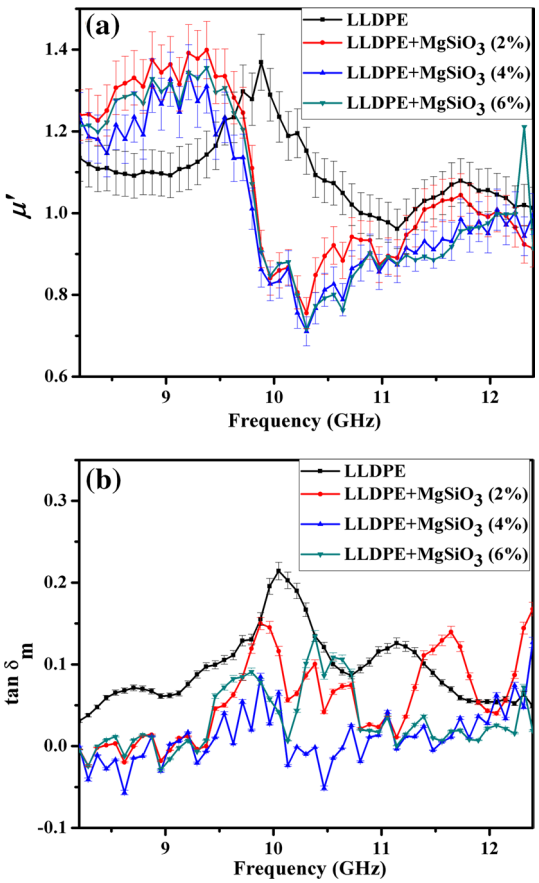

Fig. 8 (a) Real part of complex permeability and (b) Magnetic loss tangent of LLDPE-nano-$MgSiO_3$composites.

interaction. The value of tan δ_m varies within the range of 10^{-1}–10^{-5}.

The comparison of dielectric properties of LLDPE-$MgSiO_3$ composite with a few of the recently reported polymer-ceramic composites is listed in Table V.

Return Loss

By using complex permittivity and permeability data obtained from measurements conducted, return loss (R_L) of the fabricated sample is calculated. The R_L is evaluated by using Eq. 5, which is expressed as

$$\mathbf{R_L(dB)} = 20\ \mathbf{log}_{10}\left|\frac{\mathbf{Z_n}-1}{\mathbf{Z_n}+1}\right| \tag{5}$$

where

$$Z_n = \sqrt{\frac{\varepsilon_r}{\mu_r}}\tanh\left[j\left(\frac{2\pi f_p t}{c}\right)\sqrt{\varepsilon_r\mu_r}\right] \tag{6}$$

where Z_n is the input impedence w.r.t. the free space, f_p is the frequency of operation and $t = 2$ mm is the thickness

Table V Comparison of dielectric properties of proposed composite with recently reported polymer ceramic composite

Ref. no.	Composites	Optimum filler loading (%)	ε'	tan δ_e	Frequency	Applications
Ref. 6	Silicon rubber-$BaBiLiTeO_6$	0.25 %VF	6.86	4.7×10^{-2}	10 GHz	10 GHz
Ref. 7	Poyolefin-TiO_2	70 wt.%	7.03	4.2×10^{-3}	10 GHz	10 GHz
Ref. 8	PTFE-$MgTiO_3$	40 %VF	5.5	2.7×10^{-3}	10 GHz	10 GHz
Ref. 9	Polypropylene-$CaTiO_3$	80 wt.%	11.74	7×10^{-3}	X-band	X-band
Ref. 10	PTFE-(Ca,Li,Sm)TiO_3	40 %VF	7.92	1.2×10^{-3}	10 GHz	10 GHz
Ref. 11	PTFE-Si_3N_4	62 wt.%	4.03	1.4×10^{-3}	10 GHz	10 GHz
Proposed composite	LLDPE-$MgSiO_3$	6 wt.%	2.56	$\sim10^{-2}$–10^{-4}	X-band	X-band

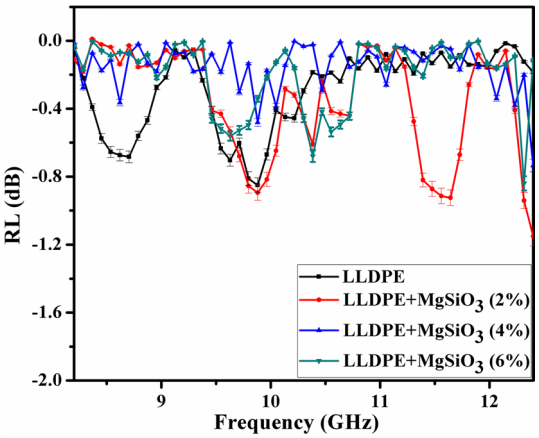

Fig. 9 Simulated return loss of LLDPE-nano-$MgSiO_3$ composites.

of the substrate and $c = 3\times10^8$m/s is the speed of light.[36] Calculated R_L of the composite substrate over the X-band is shown in Fig. 9. The figure suggests a low value of R_L as expected with a minimum value of −1 dB. At lower frequencies, a small notch is noticed in R_L, but at higher frequencies, it tends towards 0 dB. From the literature, it is observed that nanocomposites with an R_L value −45 dB is suitable for absorber application.[37] The obtained values of R_L suggests that LLDPE- nano-$MgSiO_3$ composite can be used as a substrate for high frequency microstrip patch antenna applications.

Conclusion

$MgSiO_3$ nanoparticles are synthesized by conventional solid state technique. The diffraction peaks at $2\theta = 36.81°$, 42.80°, 62.16°, 74.56° and 78.47° corresponding to the (h k l) value (1 1 2), (3 3 0), (0 6 0), (2 1 4), (4 6 4) in the XRD, confirms the presence of magnesium silicate. In the FTIR studies, the characteristic bands at 1186–1047 cm^{-1} and at 480 cm^{-1} obtained from FTIR studies correspond to the Si-O bending vibrations and Mg-O stretching vibration, respectively. The TEM images confirm the average sizes of the nano-$MgSiO_3$ as ~100 nm. Composites of LLDPE and nano-$MgSiO_3$ are prepared with 2 wt.%, 4 wt.% and 6 wt.% of $MgSiO_3$. The SEM images indicate that inclusions are uniformly dispersed in LLDPE. The complex permittivity shows a linear trend with minimal variation, which is due to the accumulation of space charge at the inclusion-polymer interfaces. As per the investigation, the composite can be utilized as microstrip patch antennas substrate, which is further confirmed by the calculated RL values. The complex permittivity and dielectric loss tangent results established in this work also fulfil the International Technology Roadmap for Semiconductors (ITRS) criteria for substrate materials.[38]

Acknowledgments The authors would like to acknowledge Prof. Nidhi S Bhattacharya, Department of Physics, Tezpur University (Central), Assam, for the support and guidance provided for carrying out some of the experimental works reported in this work.

Conflict of interest The authors declare that they have no conflict of interest.

References

1. M.T. Sebastian, R. Ubic, and H. Jantunen, Low-loss Dielectric Ceramic Materials and Their Properties. *Int. Mater. Rev.* 60, 392 (2015).
2. S. Fu, Z. Sun, P. Huang, Y. Li, and N. Hu, Some Basic Aspects of Polymer Nanocomposites: A Critical Review. *Nano Mater. Sci.* 1, 2 (2019).
3. C. Zhang, R. Zuo, J. Zhang, and Y. Wang, Structure-Dependent Microwave Dielectric Properties and Middle Temperature Sintering of Forsterite $(Mg_{1-x}Ni_x)_2SiO_4$. *J. Am. Ceram. Soc.* 98, 3 (2015).
4. P.S. Anjana, M.T. Sebastian, M.N. Suma, and P. Mohanan, Low Dielectric Loss PTFE/CeO_2 Ceramic Composites for Microwave Substrate Applications. *Int. J. Appl. Ceram. Technol.* 5, 325 (2008).
5. M.H. Ullah, M.T. Islam, M.R. Ahsan, W.N.L. Mahadi, T.A. Latef, and M.J. Uddin, A Low-cost Fiberglass Polymer Resin Dielectric Material-Based Microstrip Patch Antenna for Multiband Applications. *Sci. Eng. Compos. Mater.* 23, 447 (2016).

6. V.L. Vilesh and S. Ganesanpotti, Silicone Rubber-$BaBiLiTeO_6$ Composites: Flexible Microwave Substrates for 5G Applications. *J. Electron. Mater.* 1, 11 (2022).
7. C. Wang, B. Wu, X. Mao, T. Deng, R. Li, Y. Xu, and X. Tang, The Effects of Concentration and Particle Size of TiO_2 on the Dielectric Properties of Polyolefin-Based Microwave Substrates. *Chem. Select* 5, 1464 (2020).
8. H. Peng, H. Ren, M. Dang, Y. Zhang, Z. Gu, X. Yao, and H. Lin, The dimensional effect of $MgTiO_3$ ceramic filler on the microwave dielectric properties of PTFE/$MgTiO_3$ composite with ultra-low dielectric loss. *J. Mater. Sci. Mater. Electron.* 30, 6680 (2019).
9. V. Drishya, A.N. Unnimaya, R. Naveenraj, E.K. Suresh, and R. Ratheesh, Preparation, Characterization, and Dielectric Properties of PP/$CaTiO_3$ Composites for Microwave Substrate Applications. *J. Appl. Ceram. Technol.* 1, 810 (2016).
10. L. Zheng, J. Zhou, J. Shen, W. Chen, Y. Qi, S. Shen, and S. Li, The Dielectric Properties and Dielectric Mechanism of Perovskite Ceramic CLST/PTFE Composites. *J. Mater. Sci. Mater. Electron.* 28, 11665 (2017).
11. Y. Yuan, Z. Li, L. Cao, B. Tang, and S. Zhang, Modification of Si_3N_4 Ceramic Powders and Fabrication of Si_3N_4/PTFE Composite Substrate with High Thermal Conductivity. *Ceram. Int.* 45, 16569 (2019).
12. D. Sarmah, N.S. Bhattacharyya, and S. Bhattacharyya, Study of Graded Composite (LDPE/TIO_2) Materials as Substrate for Microstrip Patch Antennas in X-band. *IEEE Trans. Dielectr. Electr. Insul.* 20, 1845 (2013).
13. H.C. Pant, M.K. Patra, A. Verma, S.R. Vadera, and N. Kumar, Study of the Dielectric Properties of Barium Titanate-Polymer Composites. *Acta Mater.* 54, 3163 (2006).
14. A. Hoorfar and A. Perrotta, An Experimental Study of Microstrip Antennas on Very High Permittivity Ceramic Substrates and Very Small Ground Planes. *IEEE Trans. Antennas Propag.* 49, 838 (2001).
15. M.H. Ullah and M.T. Islam, Design of a Modified W-shaped Patch Antenna on Al_2O_3 Ceramic Material Substrate for Ka-Band. *Chalcogenide Lett.* 9, 61 (2012).
16. M.H. Ullah and M.T. Islam, Miniaturized Modified Circular Patch Monopole Antenna on Ceramic-Polytetrafluroethylene Composite Material Substrate. *J. Comput. Electron.* 13, 211 (2014).
17. D.D. Sandu, O. Avadanei, A. Ioachima, G. Banciua, and P. Gasner, Microstrip Patch Antenna With Dielectric Substrate. *J. Optoelectron. Adv. Mater.* 5, 1381 (2003).
18. J.A.L. Matias, I.B.T. Silva, M.E.T. Sousa, J.B.L. Oliveira, M.A. Morales, and D.R. da Silva, $(Bi_{13}Co_{11})Co_2O_{40}$-$Co_3O_4$ Nanocomposites: Synthesis, Characterization and Application as Substrate for Microstrip Patch Antenna. *Ceram. Int.* 47, 21530 (2021).
19. P.J. Gogoi, S. Bhattacharyya, and N.S. Bhattacharyya, Linear Low Density Polyethylene (LLDPE) as Flexible Substrate for Wrist and Arm Antennas in C-Band. *J. Electron. Mater.* 44, 1071 (2015).
20. K.S. Chun, S. Husseinsyah, and N.F. Syazwani, Properties of Kapok Husk-Filled Linear Low-Density Polyethylene Eco Composites: Effect of Polyethylene-Grafted Acrylic Acid. *J. Thermoplast. Compos. Mater.* 29, 1641 (2016).
21. J. He, H. Ye, S. Liu, and J. Zhao, Preparation and Properties of LLDPE/PMVS Blends. *Polym. Polym. Compos.* 14, 611 (2006).
22. M. Shafiq, T. Yasin, and S. Saeed, Synthesis and Characterization of Linear Low-Density Polyethylene/Sepiolite Nanocomposites. *J. Appl. Polym. Sci.* 123, 1718 (2012).
23. M.E. Song, J.S. Kim, M.R. Joung, and S. Nahm, Synthesis and Microwave Dielectric Properties of $MgSiO_3$ Ceramics. *J. Am. Ceram. Soc.* 91, 2747 (2008).
24. P. Dutta, B. Saikia, P.R. Alapati, and K. Borah, Linear Low-Density Polyethylene-Thermotropic Liquid Crystal Composite Substrate for High Frequency Devices: Dielectric Characterization. *J. Electron. Mater.* 50, 1434 (2021).
25. N.S.B.M. Hafidz, M.S.B.M. Rehan, and H.B. Mokhtar, Effect of Alkaline Treatment on Water Absorption and Thickness Swelling of Natural Fibre Reinforced Unsaturated Polyester Composites. *Mater. Today Proc.* 48, 720 (2022).
26. J.J. Bensch and H.J. Brynard, New Approach to Density Measurements Using Archimedes's Principle. *Nat. Phys. Sci.* 239, 96 (1972).
27. M.G. Gomes, I. Flores-Colen, F. Da Silva, and M. Pedroso, Thermal Conductivity Measurement of Thermal Insulating Mortars with EPS and Silica Aerogel by Steady-State and Transient Methods. *Constr. Build. Mater.* 172, 696 (2018).
28. S. Thomas, V. Deepu, S. Uma, P. Mohanan, J. Philip, and M.T. Sebastian, Preparation, Characterization and Properties of $Sm_2Si_2O_7$ Loaded Polymer Composites for Microelectronic Applications. *Mater. Sci. Eng. B* 163, 67 (2009).
29. A.M. Nicolson and G.F. Ross, Measurement of the Intrinsic Properties of Materials by Time Domain Techniques. *IEEE Trans. Instrum. Meas.* 19, 377 (1970).
30. G.F. Engen and C.A. Hoer, Thru-Reflect-Line: An Improved Technique for Calibrating the Dual Six-Port Automatic Network Analyzer. *IEEE Trans. Microw. Theory Technol.* 27, 987 (1979).
31. S. Ozah and N.S. Bhattacharyya, Nanosized Barium Hexaferrite in Novolac Phenolic Resin as Microwave Absorber for X-band Application. *J. Magn. Magn. Mater.* 342, 92 (2013).
32. A.F. Ahmad, Z. Abbas, S.J. Obaiys, and D.M. Abdalhadi, Improvement of Dielectric, Magnetic and Thermal Properties of OPEFB Fibre-Polycaprolactone Composite by Adding Ni-Zn Ferrite Polymers. *Polymers* 9, 12 (2017).
33. T. Karpisz, B. Salski, P. Kopyt, and J. Krupka, Measurement of Dielectrics from 20 to 50 GHz with a Fabry-Pérot Open Resonator. *IEEE Trans. Microw. Theory Tech.* 67, 1901 (2019).
34. K.L. Zhang, Z.L. Hou, L.B. Kong, H.M. Fang, and K.T. Zhan, Origin of Negative Imaginary Part of Effective Permittivity of Passive Materials Chin. *Phys. Lett.* 34, 097701 (2017).
35. E. Axelrod, A. Puzenko, Y. Haruvy, R. Reisfeld, and Y. Feldman, Negative Dielectric Loss Phenomenon in Porous Sol-Gel Glasses. *J. Non-Cryst. Solids* 352, 4166 (2006).
36. R. Kumar, H.K. Choudhary, S.P. Pawar, S. Bose, and B. Sahoo, Carbon Encapsulated Nanoscale Iron/Iron-Carbide/Graphite Particles for EMI Shielding and Microwave Absorption. *Phys. Chem. Chem. Phys.* 19, 23268 (2017).
37. H.K. Choudhary and B. Sahoo, Microwave Absorption Property of Hydrothermal Synthesized RGO/$PbFe_{12}O_{19}$ Nano Composite. *J. Converg. Technol.* 3, 918 (2017).
38. X. Huang and C. Zhi, *Polymer Nano Composite: Electrical and Thermal Properties* (Berlin: Spinger, 2016), pp. 17–18.

Publisher's Note Springer Nature remains neutral with regard to jurisdictional claims in published maps and institutional affiliations.